Chinese Physics Letters **40**, 126301 (2023) **Express Letter**

Resonant Charge Transport Assisted by the Molecular Vibration in Single-Molecule Junction from Time-Domain *ab initio* Nonadiabatic Molecular Dynamics Simulations

Yunzhe Tian(田韫哲)[1], Qijing Zheng(郑奇靖)[1*], and Jin Zhao(赵瑾)[1,2*]

[1]*Department of Physics and ICQD/Hefei National Research Center for Physical Sciences at the Microscale, University of Science and Technology of China, Hefei 230026, China*
[2]*Department of Physics and Astronomy, University of Pittsburgh, Pittsburgh, Pennsylvania 15260, USA*

(Received 4 September 2023; accepted manuscript online 27 October 2023)

Using *ab initio* nonadiabatic molecular dynamics simulation, we study the time-dependent charge transport dynamics in a single-molecule junction formed by gold (Au) electrodes and a single benzene-1,4-dithiol (BDT) molecule. Two different types of charge transport channels are found in the simulation. One is the routine non-resonant charge transfer path, which occurs in several picoseconds. The other is activated when the electronic state of the electrodes and that of the molecule get close in energy, which is referred to as the resonant charge transport. More strikingly, the resonant charge transfer occurs in an ultrafast manner within 100 fs, which notably increases the conductance of the device. Further analysis shows that the resonant charge transport is directly assisted by the B_2 and A_1 molecular vibration modes. Our study provides atomic insights into the time-dependent charge transport dynamics in single-molecule junctions, which is important for designing highly efficient single-molecule devices.

DOI: 10.1088/0256-307X/40/12/126301

In the past few years, conventional transistors that obey Moore's law have shrunk dramatically and now reach dimensions of less than 10 nm in research devices.[1,2] The further miniaturization of electronic devices remains challenging due to either technique limitations or a lack of fundamental understanding of microscopic transport mechanisms.[3] In this sense, it is remarkable that molecular-scale devices, which can be synthesized easily with abundant diversity, may permit miniaturization down to the size on the order of 1 nm,[4,5] thus, they have the potential to partly replace traditional Si-based electronic device counterparts in the future. This led to a new field of research named as molecular-scale electronics.

Theoretical modeling plays a key role in designing and optimizing functional molecular-scale electronic devices. Most industrial models have been used with Boltzmann's equation based on drift-diffusion approximation.[6–12] However, for devices at the molecular scale, when the quantum phenomena are dominant, the semi-classical Boltzmann's equation does not apply. Then, Fermi's golden rule was applied to simulate molecular devices considering the density of states (DOS) and the energy level alignment between the Fermi energy (E_F) of the electrode and the molecular energy levels.[13–18] Afterwards, the non-equilibrium Green function (NEGF) approach using many-body perturbation theory and diagrammatic theory for non-equilibrium processes was developed and widely applied in molecular device simulation.[19–26]

Considering the charge transport process at the atomic scale, it can be understood as a time-dependent dynamical process of charge carrier, in which the electron tunnels from one electrode to the other through the molecule. During this process, the vibration of the molecule will scatter the charge carrier and a real-time charge carrier dynamics simulation including the electron-vibration coupling will be essential to provide new insights into the theoretical design of molecular devices. In this sense, some wavefunction propagation methods, including time-dependent density functional theory, time-dependent Hartree–Fock theory, multi-configurational time-dependent Hartree theory, and the time-dependent density matrix renormalization group, were developed in the research area of quantum chemistry.[27–35] However, these methods are mostly used for model systems and have been seldom applied to real molecular devices.

In recent decades, the nonadiabatic molecular dynamics (NAMD) simulation approach, which combines the time-dependent Kohn–Sham (TDKS) equation with the surface hopping scheme and *ab initio* molecular dynamics, has been rapidly developed.[36–47] It accounts for electron-vibration coupling in the real-time domain and has been applied to many different materials to understand the photoexcited carrier dynamics.[48–52] In this Letter, we use the time-domain NAMD approach to simulate the real-time electron transport dynamics in a single-molecule device. We choose the well-known prototypical single-molecule device, in which two Au electrodes are connected by one benzene-1,4-dithiol (BDT) molecule, to perform the investigation. This device has been studied by many experimental and theoretical investigations using different

*Corresponding authors. Email: zqj@ustc.edu.cn; zhaojin@ustc.edu.cn
© 2023 Chinese Physical Society and IOP Publishing Ltd

methods.[53–71] We have calculated the current-voltage (I–V) curve with the electric field in the range of 0.1–0.3 V/Å and obtained the current (I) and conductance (G) in the same magnitude as the experimental measurements. Interestingly, two different types of charge transport channels are found in the simulation. The first one is the routine non-resonant charge transport channel, in which the electron relaxes to lower energy levels step by step. It occurs within several picoseconds. More strikingly, when the energy levels of the electrodes and the molecule get close, the resonant charge transfer channel is activated. In this case, the charge transfer occurs in an ultrafast manner within 100 fs, which distinctly increases the conductance of the device. The resonant charge transfer is directly associated with the excitation of the B_2 and A_1 molecular vibrational modes. This study provides unique insights into the time-dependent charge transfer dynamics in a single-molecule junction at the atomic scale.

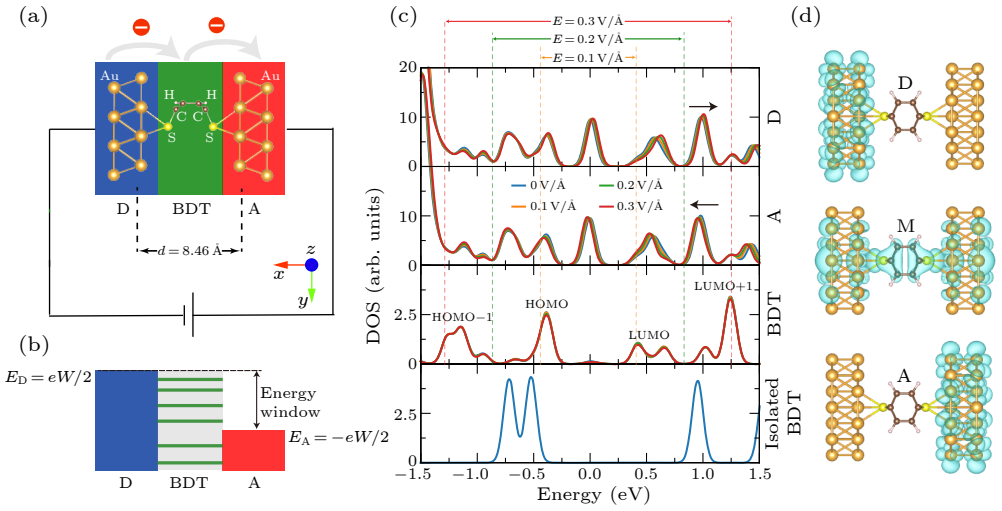

Fig. 1. (a) Schematic map of the electron transfer process in the BDT junction. (b) Energy level and energy window scheme of the molecular junction. (c) Bottom panel: DOS of isolated BDT molecule. Top three panels: pDOS of the D-electrode, A-electrode, and the BDT molecule in the BDT single-molecule junction. The blue, orange, green, and red solid lines correspond to E = 0, 0.1, 0.2, and 0.3 V/Å. The energy window is marked by vertical dashed lines. The pDOS peak movement directions of D/A-electrode are indicated by black arrows. E_F is set to be the energy reference. (d) Typical D, M, and A orbital distribution.

The molecular device we considered is formed by a single BDT molecule sandwiched between two Au electrodes terminated with the Au (111) surface as shown in Fig. 1(a). The two sulfur (S) atoms at both ends of the BDT molecule sit in the hollow position of the triangular Au atoms on the Au (111) surface, and the plane of the BDT ring is perpendicular to the Au surface. The distance between the terminal S atom and the Au surface is fixed at 2.3 Å, which is calculated by Luo *et al.*[72] Such atomic geometry of single-molecule device was widely used in previous simulations.[73–76] The geometry of the BDT molecule is relaxed first with two fixed S atoms at the experimental distance (the distance between two electrode surfaces was reported to be d = 8.46 Å in Reed's experiments[53]). Then two electrodes are added, which are simulated using cluster model. Each electrode contains two layers of 24 Au atoms, the distance between adjacent Au atoms is fixed at 2.88 Å, which is taken from the distance in the Au (111) surface.[50] The whole molecular junction is put into a 20 Å ×20 Å ×35 Å supercell, where the vacuum layer thicker than 10 Å exists between the clusters. In the Supporting Materials, we also report a simulation with the four-layer Au electrodes (48 atoms), and find that the two-layer Au electrode with 24 Au atoms provides a well-converged result. More calculation details can also be found in the Supporting Materials.

The electron transfer process through a molecular device is schematically shown in Fig. 1(a). The electron transfers from the donor electrode (labeled as D) to the acceptor electrode (labeled as A) through the BDT molecule driven by the electric field. We applied three different electric fields with E = 0.1, 0.2, and 0.3 V/Å, which are comparable to the experimental condition.[53] The projected density of states (pDOS) of the BDT molecule and Au electrodes under different electric fields are shown in Fig. 1(c). The pDOS peaks of the BDT molecule remain unchanged with increasing electric field because the molecule locates at the center of the junction, while the peaks of the D and A electrodes move slightly towards higher and lower energies [see black arrows in Fig. 1(c)], respectively, due to the electric field. To understand how the interaction with Au electrodes affects the BDT orbitals, the DOS of isolated BDT molecule is also plotted in Fig. 1(c). It can be seen that the highest occupied molecular orbital (HOMO) and HOMO-1 states hybridize with Au orbital and generate two major peaks at −1.2 and −0.4 eV below E_F, respectively. The two major peaks at 0.5 and 1.2 eV above E_F originate from the lowest unoccupied molecular orbital (LUMO) and LUMO+1 orbital, respectively. During the electron transport process, only the electronic states within the energy window are involved, as seen in Fig. 1(b). The size of the voltage window is given by $W = \boldsymbol{E}\cdot\boldsymbol{d}$, where

$\boldsymbol{E}$ is the electric field and $\boldsymbol{d}$ is the distance between the two electrodes. As a result, only the states within the energy window $[-eW/2, eW/2]$ are involved in the charge transport. The energy windows under different electric fields are also indicated by dashed lines in Fig. 1(c).

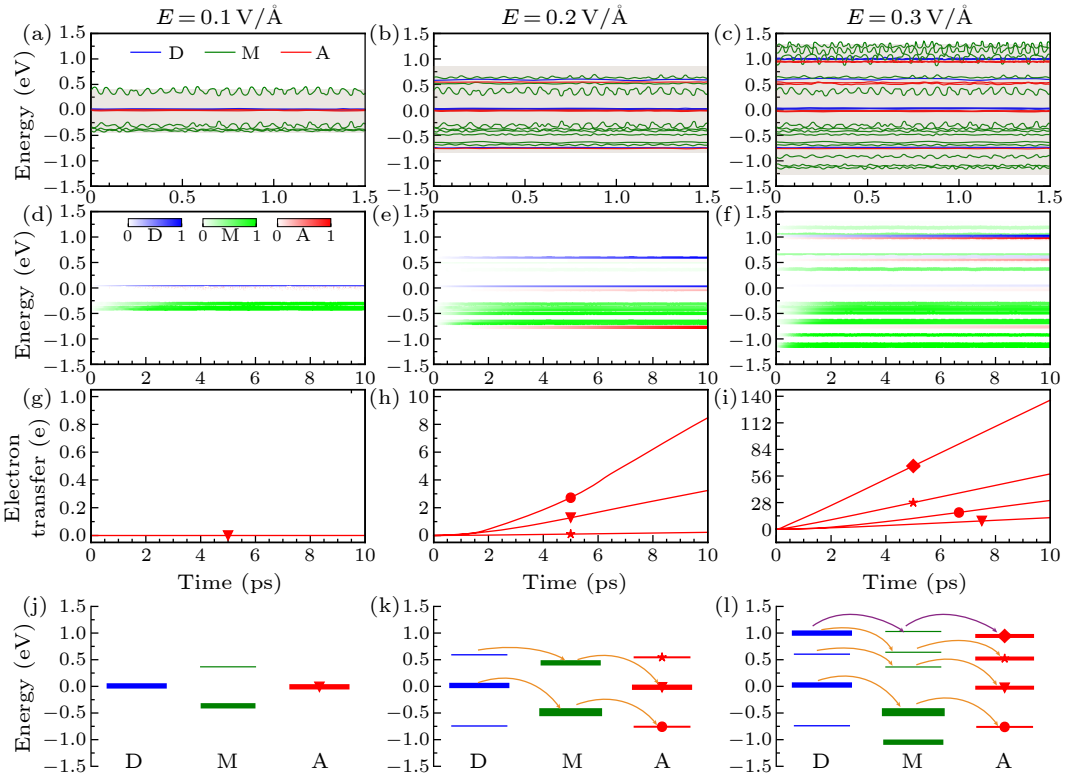

Fig. 2. (a)–(c) Time-dependent evolution of the energy states within the energy window when $E = 0.1$, 0.2, and 0.3 V/Å. The energy reference is the averaged E_F. The electronic states belonging to D, M, and A are represented by blue, green, and red colors. the gray shaded area marks the energy window. (d)–(f) Time-dependent electron decreasing on D and increasing on M and A states when $E = 0.1$, 0.2, and 0.3 V/Å, which are represented by, blue, green, and red maps and the shade of the color map suggests the magnitude of the electron population. The maximum value of D/M/A color map is the maximum electron population among all D/M/A states at 10 ps. (g)–(i) Time-dependent electron increasing on different A states, with $E = 0.1$, 0.2 and 0.3 V/Å, respectively. (j)–(l) Schematic map of the electron transfer processes in energy space, the blue, green, and red lines represent energy levels of D, M, and A, while the line thickness is proportional to the number of available molecular orbitals. The orange/purple arrows represent the non-resonant and resonant electron transfer pathways.

The NAMD simulation for charge transfer in the single BDT molecular junction is performed at 300 K. Figures 2(a)–2(c) show the time evolution of the electronic states under different electric fields within the electrostatic energy window at 300 K. The energy window is marked by the grey shaded area. Based on the above analysis, the electron transfers from the D electrode orbitals through the BDT hybridized orbitals (labeled as M) to the A electrode orbitals. Both D and A are connected to an infinite reservoir of electrons and two electrons are initialized at each D electrode orbital up to $eW/2$ energy in the NAMD simulation. In this study, we ignore the direct electron tunneling between two electrodes, namely the superexchange effects,[77,78] and only consider the D–M–A process. The influence of superexchange effects is discussed in the Supporting Materials. Orbitals belonging to D, M, and A are represented by blue, green, and red lines, where the orbital association is determined by their spatial localization (see more details in the Supporting Materials). In Fig. 1(d) we show several typical examples of D, M, and A orbital localization.

By initializing the electron at each D electrode orbital and performing the NAMD simulation, we obtain the time-dependent electron transfer on different states, as is shown in Figs. 2(d)–2(f), where blue, green, and red color maps are used to represent the electron decreasing in the D, and electron increasing in the M, and A regions, respectively. In Figs. 2(g)–2(i), we show the time-dependent charge localization on different A states with $E = 0.1$, 0.2, and 0.3 V/Å. Schematics of the charge transfer process under the three different electric fields are shown in Figs. 2(j)–2(l). As shown in Figs. 2(a), 2(d), and 2(g), with $E = 0.1$ V/Å, the energy window only ranges in $[-0.42, 0.42]$ eV. Within this region, both A states and D states locate close to the E_F, and there are no M states between them to act as electron transfer media, as shown in Fig. 2(a). In this case, the charge transfer through the D–M–A path is zero. When the electric field increases

to $E = 0.2\,\mathrm{V/Å}$, the energy window increases to $[-0.85, 0.85]\,\mathrm{eV}$ as shown in Fig. 2(b). In this case, as schematically shown in Fig. 2(k), for both D and A electrodes, two more electronic states at 0.55 and $-0.75\,\mathrm{eV}$ are involved in the charge transfer process. Electrons can transfer from the D state close to E_F to the A state at $-0.75\,\mathrm{eV}$ through the BDT HOMO state (M states range from -0.7 to $-0.3\,\mathrm{eV}$). In addition, electrons at 0.6 eV in the D electrode can transfer through the BDT LUMO state (M states range from 0.25 to 0.5 eV) to A state close to E_F. In Fig. 2(h) we plot the time-dependent electron increasing in the three A states. One can see that after a certain period of time, the electron transfer versus time correlation reaches a linear region, suggesting a stable charge transfer route is established. Since then, it takes the same amount of time (labeled as τ) to transfer an electron from D through M to one A state. For the two A states which locate close to E_F and at 0.6 eV above it, the D–M–A charge transfer τ is estimated to be 0.9 and 2.6 ps, respectively. When $E = 0.3\,\mathrm{V/Å}$, more charge transfer routes are activated, as seen in Fig. 2(l). Most strikingly, as can be seen in Fig. 2(i), the charge localization on the A states at 1.0 eV above E_F shows a rapid increase, and the stable D–M–A charge transfer time τ is estimated to be as fast as 0.1 ps. It suggests that an ultrafast charge transfer channel is activated. As can be seen in Figs. 2(c) and 2(l), there are electronic states at 1.0 eV for both D and A electrodes as well as the single BDT molecule (M). These states cross each other frequently. We propose that the resonant electron transfer occurs through these crossing states.

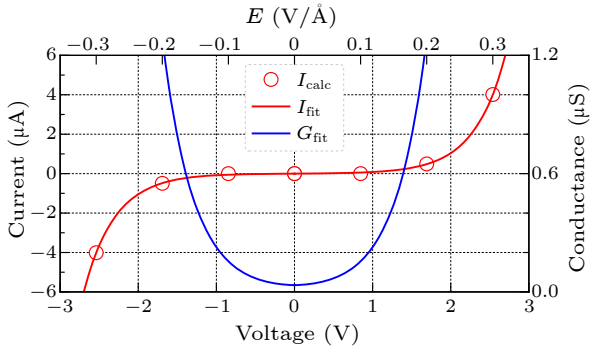

Fig. 3. I–V and G–V curves of the BDT junction. The red hollow dots are from the NAMD simulation while the red and blue solid lines correspond to the fitted current and conductance.

Based on the time-dependent electron localization, we can calculate I and G of the molecular device as

$$I = \frac{\sum_n \Delta Q_n(t)}{\Delta t}, \tag{1}$$

$$G = \frac{dI}{dV} = \frac{dI}{dE \times d}, \tag{2}$$

where $Q_n(t)$ is the time-dependent charge transfer amount in n^{th} A state (see the Supporting Materials for details), which is determined after the stable charge transfer route is established. The resulting I–V data from NAMD simulations are shown in Fig. 3 (red hollow circles), which are then fitted using a hyperbolic function. Subsequently, the G–V curve is obtained as the derivative of the I–V curve. The results are in qualitative agreement with the results reported previously.[53,79–87] The ultrafast resonant charge transfer leads to a notable increase of current when $E = 0.3\,\mathrm{V/Å}$, which is due to the activation of the resonant charge transfer channel.

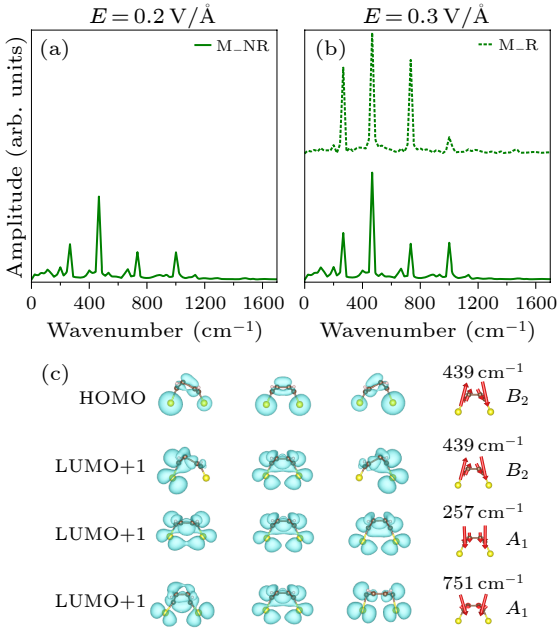

Fig. 4. [(a), (b)] FT spectra of electron-transfer-involved states for $E = 0.2$ and $0.3\,\mathrm{V/Å}$, respectively. The green lines correspond to FT spectra of the electronic states contributed by M in the non-resonant (solid lines) and resonant (dotted lines) electron transfer process, respectively. (c) The orbital distribution changes of the HOMO and LUMO+1 orbitals when the B_2 ($439\,\mathrm{cm^{-1}}$) and A_1 (751 and $257\,\mathrm{cm^{-1}}$) modes are excited.

The effects of molecular vibration on the charge transfer are naturally included. To achieve more information on how the molecular vibrations couple to the electronic states, we obtain the Fourier transform (FT) spectra of the electron-transfer-involved molecular states shown in Figs. 2(b) and 2(c). The results are shown in Figs. 4(a) and 4(b). The amplitude of the state energy fluctuation shown in Figs. 2(b) and 2(c) suggests the magnitude of the electron-vibration coupling while the corresponding peak position [Figs. 4(a) and 4(b)] indicates the vibration frequencies of the coupled modes. Compared to previous inelastic electron tunneling spectroscopy (IETS) obtained by experiments and NEGF approach,[61,88] it can be seen that peaks at $751\,\mathrm{cm^{-1}}$ and $1000\,\mathrm{cm^{-1}}$ are in agreement with both experimental and NEGF results. However, the highest frequency peak we have observed is around $1467\,\mathrm{cm^{-1}}$, which has lower frequency than what was reported. The deviation may be due to the different atomic structure used in our simulation. From the Supporting Materials, one can see that if using a BDT molecule without strain, the highest frequency peak moves to $1512\,\mathrm{cm^{-1}}$. On the other hand, the A_1 mode at $257\,\mathrm{cm^{-1}}$ in our simulation may be

correlated with the peaks below 300 cm^{-1} observed in the experiments.[61]

Trying to understand more details of how the molecular vibration affects the charge transfer, one can see that with $E = 0.2\,\mathrm{V/Å}$, the electron transfer is mainly through the HOMO orbital, and B_2 mode at 439 cm^{-1} is the major vibration mode involved in the electron transfer. The HOMO orbital is contributed by the s orbital of the S atom and the π orbital of the benzene. The B_2 mode corresponds to benzene tilting between the electrodes. Figure 4(c) shows how the HOMO changes when the B_2 mode is excited, which clearly shows how the charge transfers from D to A through the redistribution of the s orbital. When the electric field increases to $0.3\,\mathrm{V/Å}$, the resonant electron transfer channel through the LUMO+1 is activated and the A_1 modes at 751 and 257 cm^{-1} also participate besides the tilting B_2 mode. These two A_1 modes correspond to the benzene folding and fluctuating between the electrodes [Fig. 4(c)]. Their excitation affects LUMO+1 orbital distribution notably since the LUMO+1 orbital is a hybridization between the benzene π and S $3p$ orbital. The folding and fluctuating of benzene ring can change the bond length of S–C and thus influence the orbital overlap between the molecule and the electrodes. The resonant charge transfer is assisted by both the tilting B_2 and two A_1 modes. Such a kind of vibration-assisted charge transfer has also been found in two-dimensional heterojunctions as reported by Zheng *et al.*[41,89]

Our results suggest that there are two different kinds of charge transfer channels. The first one is the non-resonant electron transfer as shown by the orange arrows in Figs. 2(k) and 2(l). In this process, the electron relaxes to lower energy states step by step along the D–M–A path. When the electric field is large enough, a resonant electron transfer is observed as shown by purple arrows in Fig. 2(l), where there exist D, M, and A states that are energetically very close. It can be noted that the resonant electron transfer, which happens in 100 fs, is about one order of magnitude faster than the non-resonant electron transfer, which takes several picoseconds. The ultrafast resonant electron transfer leads to distinct increases of I and G. It was proposed that non-resonant charge transfer suffers from exponential decay with increasing molecular length.[3,7–10,90] However, the resonant charge transfer is proposed to provide a more efficient channel.[90] Our results provide new insights into the resonant charge transfer dynamics which is assisted by molecular vibration. We propose that the NAMD approach can be applied to molecular devices with longer molecules for further understanding of vibration-coupled charge transfer.

Compared with the experimental results, the I and G obtained in this work are one order of magnitude larger.[53] One possible reason is that DFT calculations always provide more delocalized wavefunctions due to the self-interaction error.[91] The adsorption structure of BDT molecule on the electrodes may also affect the results. In this work, we use $d = 8.46\,\text{Å}$, which was measured by the experiments. In this case the BDT molecule is compressed as seen in Fig. 1(a). In order to test the effects of different structures, we perform one additional calculation with $d = 10.81\,\text{Å}$. In this case the BDT molecule has a planar configuration without strain. The calculated I–V and G–V curves are given in Fig. S4. Comparing with Fig. 3 in the main text, one can see that the planar BDT molecule without strain has higher conductance, which is consistent with previous investigations.[91–93] Certainly, it will be interesting to further study how the different adsorption structure affects the single molecule device conductance.

We have calculated the same molecular junction using the NEGF approach and have achieved larger current comparing with the NAMD simulation. The results are shown in the Supporting Materials. The difference in current values may be due to the fundamental difference between NEGF and NAMD, where the NEGF is based on the perturbation theory while the NAMD approach is based on real-time TDKS. Another possible reason is the treatment of the Au electrode. It should also be noted that the Au cluster used in this work does not fully reproduce the electronic structure of the electrode. In the Supporting Materials we have compared the pDOS of the cluster model with the infinite size electrodes using periodic condition. It can be seen that the energy positions of HOMO−1, HOMO, LUMO, LUMO+1 orbitals do not change much. The molecule-electrode hybridization becomes stronger when the infinite size electrodes are applied. Therefore, we propose that the simulation with the cluster model may underestimate the current. However, in the NAMD framework, the charge transfer is proportional to the orbital overlap between the electrodes and the molecule. We propose that the Au cluster can capture the orbitals which have strong overlap with the molecule, and the simulation with the four-layer Au electrodes (48 atoms) and two-layer Au electrode with 24 Au atoms provides a well-converged result (Fig. S1). Certainly, it is interesting to develop new approaches in the NAMD framework which can simulate the boundary condition more accurately.

Finally, we briefly state how we understand the difference of NAMD from NEGF. The NEGF approach is based on the framework of many-body perturbation theory, while NAMD is based on the time-dependent Schrödinger equation. When the electric field is applied, there is a potential difference between two electrodes and the electrons will relax from one electrode to the other, and NAMD can directly simulation such relaxation using TDKS and surface hopping. NEGF approach has achieved great success in describing the charge transport problem. Here we prove that such problems may also be studied by NAMD simulation, which can provide the time-dependent charge transfer information. We propose that it can be used to study the ultrafast opto-electronic devices if a time-dependent optical pulse is included in the simulation in addition to the electric field, which will be difficult for the NEGF approach. Moreover, the atomic vibration and vibration-electron coupling are naturally involved in the simulation, and thus the temperature dependence of the device can be easily investigated. Lastly, since the NAMD approach has been also applied to investigate the spin-polarized carrier dynamics,[40,44–46,51,94,95] this approach can be easily

extended and be applied to study spintronic devices.

To conclude, using *ab initio* NAMD simulation, we have investigated the time-dependent charge transfer dynamics in single-molecule junction formed by BDT molecule and Au electrodes. We discover two types of charge transport channels. The routine non-resonant charge transfer happens within several picoseconds. Strikingly, the ultrafast resonant charge transfer within 100 fs is activated when the electrodes and molecule have very close energy levels. It is directly coupled to the A_1 and B_2 molecular vibration modes. This work provides new insights into the charge transfer dynamics in a single-molecule junction and the *ab initio* NAMD approach proposed in this work plays an important role in designing the highly efficient single-molecule devices.

Acknowledgments. J.Z. acknowledges the support of the Strategic Priority Research Program of the Chinese Academy of Sciences (Grant No. XDB0450101), the National Key R&D Program of China (Grant No. 2017YFA0204904), the National Natural Science Foundation of China (Grant Nos. 11974322 and 12125408), and the Informatization Plan of Chinese Academy of Sciences (Grant No. CAS-WX2021SF-0105). Q.Z. acknowledges the National Natural Science Foundation of China (Grant No. 12174363). Calculations were performed at Hefei Advanced Computing Center, Supercomputing Center at USTC, and ORISE Supercomputer. H.P. acknowledges support from the National Science Foundation (Grant No. CHE-2102601).

References

[1] Chen Y Q *et al.* 2021 *Int. J. Extreme Manuf.* **3** 032002
[2] Xiang D *et al.* 2016 *Chem. Rev.* **116** 4318
[3] Haedler A T *et al.* 2015 *Nature* **523** 196
[4] Tsutsui M and Taniguchi M 2012 *Sensors* **12** 7259
[5] Song H *et al.* 2011 *Adv. Mater.* **23** 1583
[6] Fang X Y *et al.* 2015 *Phys. Lett. A* **379** 2245
[7] Mortazavi B *et al.* 2021 *Comput. Phys. Commun.* **258** 107583
[8] Amin V P and Stiles M D 2016 *Phys. Rev. B* **94** 104420
[9] Li W *et al.* 2014 *Comput. Phys. Commun.* **185** 1747
[10] Gu X K and Yang R G 2014 *Appl. Phys. Lett.* **105** 131903
[11] Hosur P *et al.* 2012 *Phys. Rev. Lett.* **108** 046602
[12] Long M Q *et al.* 2011 *ACS Nano* **5** 2593
[13] Dal F S *et al.* 2018 *J. Phys. Chem. C* **122** 8517
[14] Zhao Y and Liang W Z 2012 *Chem. Soc. Rev.* **41** 1075
[15] Esfarjani K *et al.* 2011 *Phys. Rev. B* **84** 085204
[16] Akturk A and Goldsman N 2008 *J. Appl. Phys.* **103** 053702
[17] Hennebicq E *et al.* 2005 *J. Am. Chem. Soc.* **127** 4744
[18] Fischetti M V 1991 *IEEE Trans. Electron. Devices* **38** 634
[19] Smidstrup S *et al.* 2020 *J. Phys.: Condens. Matter* **32** 015901
[20] Enkovaara J *et al.* 2010 *J. Phys.: Condens. Matter* **22** 253202
[21] Xue Y Q *et al.* 2002 *Chem. Phys.* **281** 151
[22] Datta S 2000 *Superlattices Microstruct.* **28** 253
[23] Lake R *et al.* 1997 *J. Appl. Phys.* **81** 7845
[24] Zelovich T *et al.* 2017 *J. Chem. Phys.* **146** 092331
[25] Chen L P *et al.* 2014 *J. Phys. Chem. C* **118** 20009
[26] Brenes M *et al.* 2020 *Phys. Rev. X* **10** 031040
[27] Li Y H and Ullrich C A 2008 *J. Chem. Phys.* **129** 044105
[28] Moccia R 1973 *Int. J. Quantum Chem.* **7** 779
[29] Nest M *et al.* 2005 *J. Chem. Phys.* **122** 124102
[30] Luo H G *et al.* 2003 *Phys. Rev. Lett.* **91** 049701
[31] Miranda R P *et al.* 2011 *J. Chem. Phys.* **134** 244102
[32] Heidrich-Meisner F *et al.* 2009 *Phys. Rev. B* **79** 235336
[33] Manthe U *et al.* 1992 *J. Chem. Phys.* **97** 3199
[34] Meyer H D *et al.* 1990 *Chem. Phys. Lett.* **165** 73
[35] McLachlan A D and Ball M A 1964 *Rev. Mod. Phys.* **36** 844
[36] Cui G L and Thiel W 2014 *J. Chem. Phys.* **141** 124101
[37] Akimov A V and Prezhdo O V 2013 *J. Chem. Theory Comput.* **9** 4959
[38] Akimov A V and Prezhdo O V 2014 *J. Chem. Theory Comput.* **10** 789
[39] Li W *et al.* 2018 *ACS Energy Lett.* **3** 2159
[40] Prezhdo O V 2021 *Acc. Chem. Res.* **54** 4239
[41] Zheng Q J *et al.* 2017 *Nano Lett.* **17** 6435
[42] Xie Y *et al.* 2019 *J. Mater. Chem. A* **7** 27484
[43] Chu W B *et al.* 2020 *J. Phys. Chem. Lett.* **11** 10073
[44] Jiang X *et al.* 2021 *Sci. Adv.* **7** eabf3759
[45] Zheng Z F *et al.* 2022 *Phys. Rev. B* **105** 085142
[46] Chu W B *et al.* 2022 *Sci. Adv.* **8** eabo2675
[47] Yin Y Y *et al.* 2022 *Adv. Funct. Mater.* **32** 2206952
[48] Li W *et al.* 2021 *Nanoscale* **13** 10239
[49] Long R *et al.* 2017 *Wiley Interdiscip. Rev.-Comput. Mol. Sci.* **7** e1305
[50] Wang C *et al.* 2015 *Sci. Rep.* **5** 10213
[51] Zheng Q J *et al.* 2019 *Wiley Interdiscip. Rev.-Comput. Mol. Sci.* **9** e1411
[52] Zheng Z F *et al.* 2021 *Acta Phys. Sin.* **70** 177101 (in Chinese)
[53] Reed M A *et al.* 1997 *Science* **278** 252
[54] Fatemi V *et al.* 2011 *Nano Lett.* **11** 1988
[55] Demir F and Kirczenow G 2012 *J. Chem. Phys.* **137** 094703
[56] Bruot C *et al.* 2012 *Nat. Nanotechnol.* **7** 35
[57] Baheti K *et al.* 2008 *Nano Lett.* **8** 715
[58] Arroyo C R *et al.* 2011 *J. Am. Chem. Soc.* **133** 14313
[59] Aradhya S V *et al.* 2012 *Nat. Mater.* **11** 872
[60] Xiao X Y *et al.* 2004 *Nano Lett.* **4** 267
[61] Song H *et al.* 2009 *Nature* **462** 1039
[62] Garcia-Lastra J M and Thygesen K S 2011 *Phys. Rev. Lett.* **106** 187402
[63] Garcia-Lastra J M *et al.* 2009 *Phys. Rev. B* **80** 245427
[64] French W R *et al.* 2013 *Nanoscale* **5** 3654
[65] French W R *et al.* 2013 *J. Phys. Chem. Lett.* **4** 887
[66] Flores F *et al.* 2009 *Phys. Chem. Chem. Phys.* **11** 8658
[67] Filippetti A *et al.* 2011 *Phys. Rev. B* **84** 195127
[68] Ferretti A *et al.* 2005 *Phys. Rev. B* **72** 125114
[69] Andreoni W *et al.* 2000 *Int. J. Quantum Chem.* **80** 598
[70] Yamada A *et al.* 2016 *Nano Lett.* **16** 6092
[71] Pontes R B *et al.* 2006 *J. Am. Chem. Soc.* **128** 8996
[72] Luo Y *et al.* 2002 *J. Chem. Phys.* **117** 10283
[73] Xue Y Q *et al.* 2001 *J. Chem. Phys.* **115** 4292
[74] Di Ventra M *et al.* 2000 *Phys. Rev. Lett.* **84** 979
[75] Yaliraki S N *et al.* 1999 *J. Chem. Phys.* **111** 6997
[76] Tian W D *et al.* 1998 *J. Chem. Phys.* **109** 2874
[77] Anderson P W 1950 *Phys. Rev.* **79** 350
[78] Halpern J and Orgel L E 1960 *Discuss. Faraday Soc.* **29** 32
[79] Kim Y *et al.* 2011 *Nano Lett.* **11** 3734
[80] Ghosh S *et al.* 2005 *Appl. Phys. Lett.* **87** 233509
[81] Haiss W *et al.* 2008 *J. Phys.: Condens. Matter* **20** 374119
[82] Tian J H *et al.* 2010 *ChemPhysChem.* **11** 2745
[83] Lörtscher E *et al.* 2007 *Phys. Rev. Lett.* **98** 176807
[84] Yeganeh S *et al.* 2009 *Nano Lett.* **9** 1770
[85] Tian J H *et al.* 2010 *Nanotechnology* **21** 274012
[86] Yang Y *et al.* 2016 *Nano Res.* **9** 560
[87] Ojeda J H *et al.* 2020 *RSC Adv.* **10** 32127
[88] Lü J T *et al.* 2014 *Phys. Rev. B* **89** 081405
[89] Zheng Q J *et al.* 2018 *Phys. Rev. B* **97** 205417
[90] Zang Y P *et al.* 2018 *J. Am. Chem. Soc.* **140** 13167
[91] Souza A D M *et al.* 2014 *Nanoscale* **6** 14495
[92] Ning Z Y *et al.* 2014 *Front. Phys.* **9** 780
[93] Gao W *et al.* 2009 *Appl. Surf. Sci.* **255** 9259
[94] Zhao C Y *et al.* 2017 *Phys. Rev. B* **96** 134308
[95] Lei Y L *et al.* 2022 *J. Phys. Chem. Lett.* **13** 4840